

First Dark Matter Results from the XENON100 Experiment

E. Aprile,¹ K. Arisaka,² F. Arneodo,³ A. Askin,⁴ L. Baudis,⁴ A. Behrens,⁴ E. Brown,² J. M. R. Cardoso,⁵ B. Choi,¹ D. B. Cline,² S. Fattori,³ A. D. Ferella,⁴ K.-L. Giboni,¹ K. Hugenberg,⁶ A. Kish,⁴ C. W. Lam,² J. Lamblin,⁷ R. F. Lang,¹ K. E. Lim,¹ J. A. M. Lopes,⁵ T. Marrodán Undagoitia,⁴ Y. Mei,⁸ A. J. Melgarejo Fernandez,¹ K. Ni,⁹ U. Oberlack,⁸ S. E. A. Orrigo,⁵ E. Pantic,² G. Plante,^{1,*} A. C. C. Ribeiro,⁵ R. Santorelli,⁴ J. M. F. dos Santos,⁵ M. Schumann,^{4,8} P. Shagin,⁸ A. Teymourian,² D. Thers,⁷ E. Tziaferi,⁴ H. Wang,² and C. Weinheimer⁶

(XENON100 Collaboration)

¹Physics Department, Columbia University, New York, NY 10027, USA

²Physics & Astronomy Department, University of California, Los Angeles, USA

³INFN Laboratori Nazionali del Gran Sasso, Assergi, 67100, Italy

⁴Physics Institute, University of Zürich, Winterthurerstr. 190, CH-8057, Switzerland

⁵Department of Physics, University of Coimbra, R. Larga, 3004-516, Coimbra, Portugal

⁶Institut für Kernphysik, Westfälische Wilhelms-Universität Münster, 48149 Münster, Germany

⁷SUBATECH, Ecole des Mines de Nantes, Université de Nantes, CNRS/IN2P3, Nantes, France

⁸Department of Physics, Rice University, Houston, TX 77005 - 1892, USA

⁹Department of Physics, Shanghai Jiao Tong University, Shanghai, 200240, China

The XENON100 experiment, in operation at the Laboratori Nazionali del Gran Sasso in Italy, is designed to search for dark matter WIMPs scattering off 62 kg of liquid xenon in an ultra-low background dual-phase time projection chamber. In this letter, we present first dark matter results from the analysis of 11.17 live days of non-blind data, acquired in October and November 2009. In the selected fiducial target of 40 kg, and within the pre-defined signal region, we observe no events and hence exclude spin-independent WIMP-nucleon elastic scattering cross-sections above $3 \times 10^{-44} \text{ cm}^2$ for $50 \text{ GeV}/c^2$ WIMPs at 90% confidence level. Below $20 \text{ GeV}/c^2$, this result challenges the interpretation of the CoGeNT and DAMA signals as being due to spin-independent, elastic, light mass WIMP interactions.

PACS numbers: 95.35.+d, 14.80.Ly, 29.40.-n, 95.55.Vj

Keywords: Dark Matter, Direct Detection, Xenon

A vast array of observational evidence suggests that 83% of the matter in the universe is in some unknown form called dark matter [1]. Extensions of the Standard Model of particle physics that aim at addressing some of the puzzles associated with the electroweak scale predict stable Weakly Interacting Massive Particles (WIMPs), that can be thermally produced in the early universe and become ideal dark matter candidates [2]. One method to detect WIMPs is to measure the energy they deposit in a detector by scattering off target nuclei.

XENON100 is a new ultra-low background detector developed to continue the XENON dark matter search program with liquid xenon (LXe) as WIMP target and detection medium. Like XENON10 [3], it is a three-dimensional (3D) position-sensitive dual-phase (liquid/gas) time projection chamber (TPC) filled with ultra-pure LXe. Particle interactions in the sensitive LXe volume are measured with two arrays of photomultiplier tubes (PMTs), which simultaneously detect the primary scintillation (S1) and the ionization signal (S2), via the proportional scintillation mechanism [4]. The 3D event localization allows “fiducialization” of the TPC, keeping only an inner volume in which the background rate is drastically reduced. The different ionization density of nuclear recoils, from neutrons or WIMPs, and electronic recoils, from γ or β backgrounds, leads to a different S2/S1 ratio, which can be used to discriminate the two

types of recoils.

The detector uses 161 kg of LXe, divided in two concentric cylindrical volumes. These are physically and optically separated from each other by polytetrafluoroethylene (PTFE) panels on the side, a PMT array on the bottom, and a stainless steel diving bell on the top. The bell allows the inner liquid level to be set independently of the outer one. The PTFE panels define the TPC with 30.5 cm diameter and 30.6 cm height, acting also as an efficient UV reflector. Four stainless steel meshes provide the electric field to drift ionization electrons in the liquid, extract them to the gas phase, and accelerate them to produce proportional scintillation. A drift field of 530 V/cm has been used for the measurements reported here.

The PMTs are 2.5 cm \times 2.5 cm metal-channel type (R8520-AL) specifically developed in collaboration with Hamamatsu Co. for operation in LXe, with a quantum efficiency of about 30% at 178 nm and with low intrinsic radioactivity ($< 1 \text{ mBq}/\text{PMT}$ in $^{238}\text{U}/^{232}\text{Th}$). The 80 PMT array at the bottom of the TPC is immersed in the liquid to efficiently detect the S1 signal, while another array of 98 PMTs is placed in the xenon gas above the anode so that the hit pattern of an S2 signal can be used to reconstruct the event position in (x, y) . The interaction depth (z) in the detector can be computed from the time difference between S1 and S2 pulses with

resolution < 2 mm. The outermost LXe volume is used as an active veto, instrumented with 64 PMTs. The energy threshold of the veto has been measured to be better than 200 keV_{ee} (keV electron-equivalent). The signals from all 242 PMTs are digitized at 100 MS/s and 40 MHz bandwidth. The trigger is provided by the summed signal of 84 central PMTs, low-pass filtered with 1 MHz. Given the strong amplification in the gas proportional region, at low energies the trigger is given by the S2 pulse, with an efficiency $> 99\%$ above 300 photoelectrons (PE).

The detector has been deployed underground at the Laboratori Nazionali del Gran Sasso (LNGS), where the muon flux is reduced by a factor 10^6 , thanks to the average 3600 m water equivalent of rock overburden. The LXe is contained in a double walled, vacuum insulated, stainless steel cryostat. A 200 W pulse tube refrigerator (PTR) continuously liquifies the gas circulated through a hot getter and maintains the liquid at -91°C . The PTR system is installed outside a passive shield to achieve a lower radioactive background in the target. This shield consists of a 20 cm thick layer of lead and a 20 cm thick layer of polyethylene within, to attenuate the background from external γ -rays and neutrons, respectively. The shield structure rests on a 25 cm thick slab of polyethylene and is surrounded on the top and three sides by a 20 cm thick water layer to lower the background contribution from neutrons from the cavern rock. A 5 cm thick layer of copper covers the inner surface of the polyethylene to attenuate the gamma background due to its radioactivity. Calibration sources (^{57}Co , ^{60}Co , ^{137}Cs , $^{241}\text{AmBe}$) are inserted through a copper tube which penetrates the shield and circles around the detector in the middle of the drift region.

The gas used for this experiment has been processed through a distillation column to reduce the ^{85}Kr background to $33 \mu\text{Bq}/\text{kg}$, as measured with delayed β - γ coincidences [5]. With an isotopic abundance of 10^{-11} , this ^{85}Kr contamination corresponds to 143^{+130}_{-90} ppt (mol/mol), at 90% confidence, of natural Kr.

PMT gains are measured in the single PE regime using light emitting diodes (LEDs) outside the detector vessel, connected to optical fibers which illuminate the TPC and veto volumes. The PMT gains, equalized to 1.9×10^6 at the beginning of the run, are regularly monitored and are stable within $\pm 2\%$ (σ/μ).

Event positions are calculated using three independent algorithms, based on χ^2 minimization, Support Vector Machine (SVM) regression, and a Neural Network (NN). We take the PMT gains into account and correct for non-uniformities of the drift field as inferred from a finite element simulation. The three algorithms give consistent results for radii $r < 14$ cm with an (x, y) resolution better than 3 mm, as measured with a collimated ^{57}Co source. This motivated the choice, for the present analysis, of a 40 kg fiducial volume as a cylinder of radius 13.5 cm and height 24.3 cm.

Corrections for the spatial dependence of the S1 light collection in the TPC are obtained by irradiating the detector at different azimuthal positions with an external ^{137}Cs source and computing the average light yield in $1 \text{ cm} \times 2.5 \text{ cm}$ (r, z) cells. The average light yield of the whole TPC for ^{137}Cs 662 keV_{ee} γ -rays is 1.57 PE/keV_{ee} at a field of 530 V/cm. The spatial correction is also inferred using 40 keV_{ee} γ -rays produced during the calibration of the detector with an external $^{241}\text{AmBe}$ source, via the inelastic reaction $^{129}\text{Xe} (n, n' \gamma) ^{129}\text{Xe}$. These γ -rays are more uniformly distributed in the sensitive volume due to the larger neutron mean free path. In addition, 164 keV_{ee} γ -rays from the decay of metastable ^{131m}Xe , following the same neutron calibration, are used to infer the spatial dependence of S1 signals. The corrections inferred from these independent calibrations differ by less than 3% and improve the energy resolution (σ/E) at 662 keV_{ee} from 24% to 13% using the scintillation signal alone.

Calibrations with ^{137}Cs were taken daily during the data taking presented here, to infer the electron lifetime and to subsequently correct the S2 signal for its drift time dependence. The electron lifetime increased from $154 \mu\text{s}$ to $192 \mu\text{s}$, corresponding to an average S2 z -correction of 75% to 60%, respectively. The S2 signal is also corrected for its (x, y) variation, mostly due to light collection effects near the edge of the TPC. This dependence is determined using the 40 keV_{ee} inelastic reaction calibration data and computing the proportional scintillation light yield in $2 \text{ cm} \times 2 \text{ cm}$ (x, y) cells. No significant differences ($< 2\%$) were observed between corrections obtained using other calibration datasets of various γ -ray energies (164 keV_{ee}, 662 keV_{ee}). The energy resolution (σ/E) at 662 keV_{ee} using the S2 signal alone is improved from 7.3% to 6.5% after applying the S2 spatial corrections.

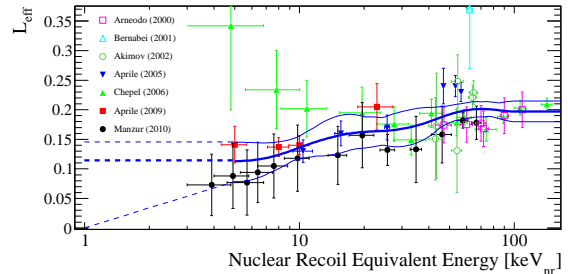


FIG. 1: Global fit to all \mathcal{L}_{eff} measurements between 5 keV_{nr} and 100 keV_{nr}, together with 90% confidence contours (solid lines) and extrapolations to lower energies (dashed lines).

The nuclear-recoil equivalent energy, E_{nr} , in LXe is conventionally computed from the scintillation signal, S_1 , using $E_{\text{nr}} = S_1/L_y \cdot 1/\mathcal{L}_{\text{eff}} \cdot S_{\text{ee}}/S_{\text{nr}}$, where \mathcal{L}_{eff} is the scintillation efficiency of nuclear recoils relative to that of 122 keV_{ee} γ -rays at zero field, and S_{ee} and S_{nr} are the electric field scintillation quenching factors for electronic and nuclear recoils, respectively with measured values of 0.58 and 0.95 [6]. Since 122 keV_{ee} γ -rays cannot penetrate far in the sensitive volume, their light yield L_y at 530 V/cm is calculated from a fit to the mea-

sured scintillation yield of several other γ -ray lines: the 40 keV_{ee} and 80 keV_{ee} lines from inelastic neutron scatters on ^{129}Xe and ^{131}Xe , respectively, the 164 keV_{ee} and 236 keV_{ee} lines from the decays of the metastable $^{131\text{m}}\text{Xe}$ and $^{129\text{m}}\text{Xe}$ isotopes, respectively, and the 662 keV_{ee} line from ^{137}Cs . The value thus obtained is $L_y(122 \text{ keV}_{\text{ee}}) = (2.20 \pm 0.09) \text{ PE/keV}_{\text{ee}}$. The most recent measurements of \mathcal{L}_{eff} in LXe [7, 8] extend below 10 keV_{nr}, as shown in Fig. 1, together with earlier data [9]. The energy dependence of \mathcal{L}_{eff} is parameterized by a global cubic-spline fit to all data in the energy range with at least two measurements (5–100 keV_{nr}). The spline knots are fixed at 5, 10, 25, 50 and 100 keV_{nr} and \mathcal{L}_{eff} is assumed constant below 5 keV_{nr} to reflect the trend seen in Aprile *et al.* [7] and Sorensen *et al.* [10]. The lower 90% confidence contour for \mathcal{L}_{eff} is also shown in Fig. 1, along with a logarithmic extrapolation to zero scintillation near 1 keV_{nr}, following the trend in Manzur *et al.* [8].

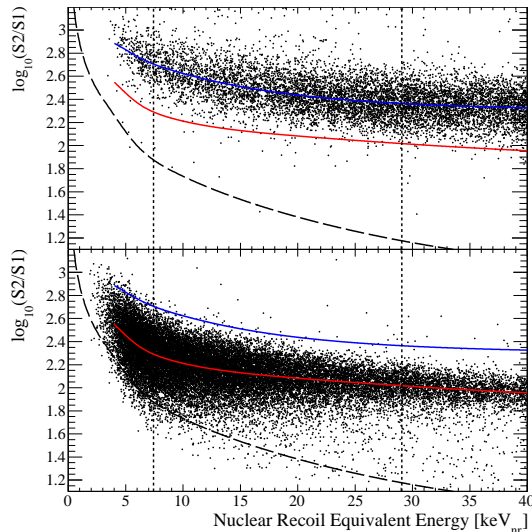


FIG. 2: Electronic (top) and nuclear (bottom) recoil bands from ^{60}Co and $^{241}\text{AmBe}$ calibration data, respectively, using the discrimination parameter $\log_{10}(\text{S2}/\text{S1})$ as a function of nuclear recoil equivalent energy (keV_{nr}). Colored lines correspond to the median $\log_{10}(\text{S2}/\text{S1})$ values of the electronic (blue) and nuclear (red) recoil bands. The energy window 7.4 – 29.1 keV_{nr} (4 – 20 PE) chosen for the WIMP search is indicated (vertical dashed lines) as well as the S2 software threshold of 300 PE (long dashed line).

Data selection criteria are motivated by the physical properties of xenon scintillation light, the characteristics of proportional light signals, and the expected WIMP-induced single-scatter nuclear-recoil signature. Cuts were developed and tested on calibration data, specifically on low energy electronic recoils from Compton scattered ^{60}Co γ -rays and nuclear recoils from $^{241}\text{AmBe}$. In particular, a two-fold PMT coincidence is required in a 20 ns window for the S1 signal and events which contain more than a single S1-like pulse are discarded. This allows true low energy events to be distinguished from events with random single photoelectrons from PMTs or accidental coincidences. For the S2 signal, a lower threshold

of 300 PE is set, corresponding to about 15 ionization electrons, and events are required to contain only one S2 pulse above this threshold. This rejects events with multiple scatters at different z positions. In addition, the width of the S2 pulse is required to be consistent with what is expected from the inferred drift time due to diffusion of the electron cloud [11]. Events that deposit energy in the veto volume in coincidence with the S1 signal in the TPC are also discarded. The regions of the digitized waveform away from S1 or S2 pulses are required to be free of extraneous PMT signals or noise. Finally, events outside the pre-defined fiducial volume are rejected.

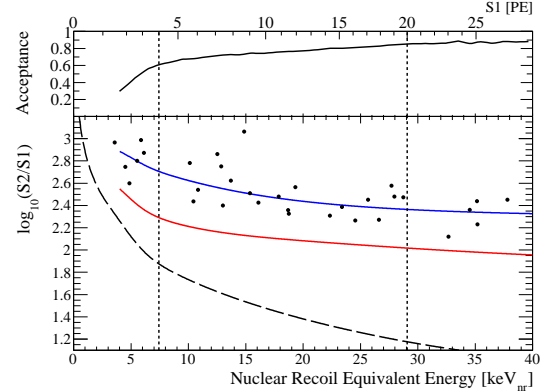


FIG. 3: Cut acceptance (top) and $\log_{10}(\text{S2}/\text{S1})$ (bottom) as functions of nuclear recoil energy for events observed in the 40 kg fiducial volume during 11.17 live days. 22 events are observed within the 7.4 – 29.1 keV_{nr} energy window, but none of them fall in the pre-defined signal acceptance region below the nuclear recoil median (red line). Lines as in figure 2.

Background rejection in XENON100 is achieved through a combination of volume fiducialization and the identification of recoil species based on the ratio S2/S1 for electronic and nuclear recoils. Accurate knowledge of the response to both types of recoils is essential to define the signal region, to determine the signal acceptance, and to predict the expected leakage into the signal region. Statistics for the low energy electronic recoil calibration are accumulated at regular intervals with a 1 kBq ^{60}Co source. The response of XENON100 to elastic nuclear recoils was obtained by irradiating the detector with a 220 n/s $^{241}\text{AmBe}$ source for 72 h. Fig. 2 shows the $\log_{10}(\text{S2}/\text{S1})$ distribution of single scatter electronic and nuclear recoils as a function of nuclear recoil energy. The behavior of the electronic and nuclear recoil bands measured with this large TPC is similar to what was previously observed with a small prototype [6] and with XENON10 [3, 10].

A first dark matter analysis has been carried out, using 11.17 live days of background data, taken from October 20th to November 12th 2009, prior to the neutron calibration. Although this was not a blind analysis, all the event selection criteria were defined on calibration data. The upper end of the energy range of 7.4 – 29.1 keV_{nr} (4 – 20 PE) is chosen to correspond approximately to

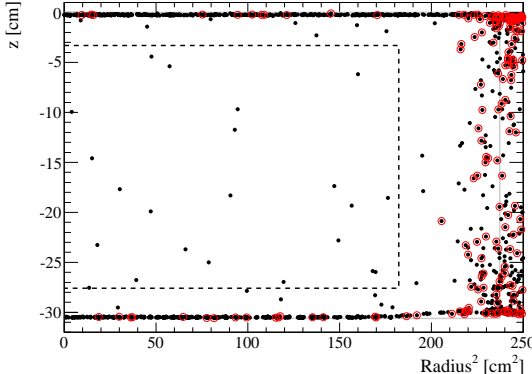


FIG. 4: Distribution of all events (dots) and events below the nuclear recoil median (red circles) in the TPC (grey line) observed in the $7.4 - 29.1 \text{ keV}_{\text{nr}}$ energy range during 11.17 live days. No events below the nuclear recoil median are observed within the 40 kg fiducial volume (dashed).

the one used for the XENON10 blind analysis [3], after recomputing the corresponding nuclear recoil equivalent energy using the new \mathcal{L}_{eff} parametrization from the global fit, shown in Fig. 1. The lower bound is motivated by the fact that the acceptance of the S1 two-fold coincidence requirement is $> 90\%$ above 4 PE. The $\log_{10}(S2/S1)$ upper and lower bounds of the signal region are respectively chosen as the median of the nuclear recoil band and the 300 PE S2 threshold. No signal candidate event is observed as shown in Fig. 3. The cumulative software cut acceptance for single scatter nuclear recoils is conservatively estimated to vary between 60% (at $7.4 \text{ keV}_{\text{nr}}$) and 85% (at $29.1 \text{ keV}_{\text{nr}}$) by considering all events removed by only a single cut to be valid events (Fig. 3). At 50% nuclear recoil acceptance, the electronic recoil discrimination based on $\log_{10}(S2/S1)$ is above 99%, predicting < 0.2 background events in the pre-defined WIMP signal region. The observed rate, spectrum, and spatial distribution (Fig. 4) agree well with a GEANT4 Monte Carlo simulation of the entire detector.

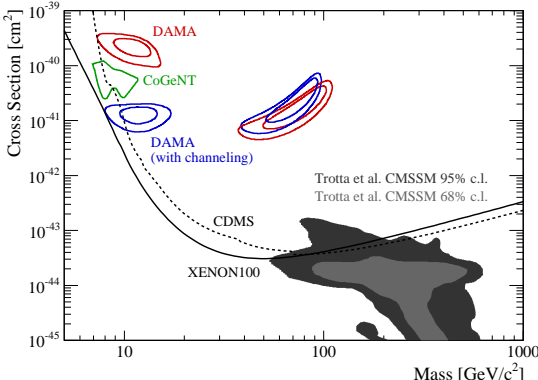


FIG. 5: 90% confidence limit on the spin-independent elastic WIMP-nucleon cross section (solid line), together with the best limit to date from CDMS (dashed) [12], expectations from a theoretical model [13], and the areas favored by CoGeNT (green) [14] and DAMA (blue/red) (3σ , 90%) [15].

An upper limit on the WIMP-nucleon elastic scatter-

ing cross section is derived based on the standard halo assumptions [16], taking into account an S1 resolution dominated by Poisson fluctuations, and with \mathcal{L}_{eff} from the global fit, assumed constant below $5 \text{ keV}_{\text{nr}}$. Fig. 5 shows the resulting 90% confidence upper limit. This limit has a minimum at a cross section of $3 \times 10^{-44} \text{ cm}^2$ for a WIMP mass of $50 \text{ GeV}/c^2$, using a spectrum-averaged exposure of $161 \text{ kg} \cdot \text{days}$. The interpretation of the CoGeNT [14] and DAMA [15] signals as being due to light mass WIMPs is difficult to reconcile with our data. Even with the 90% confidence lower contour for \mathcal{L}_{eff} in Fig. 1 (which raises our *a priori* chosen threshold of 4 PE from $7.4 \text{ keV}_{\text{nr}}$ to $9.1 \text{ keV}_{\text{nr}}$), most of the CoGeNT favored parameter space is excluded. However, our data extends below 4 PE, although at reduced acceptance. For a $7 \text{ GeV}/c^2$ WIMP, at the lower edge of the CoGeNT region, with a cross section of $5 \times 10^{-41} \text{ cm}^2$, we would expect to find 3.6 events above 3 PE ($7.1 \text{ keV}_{\text{nr}}$). No events are observed, leading to a rejection of the light WIMP hypothesis with $> 90\%$ confidence even in this case. This initial result, based on only 11.17 live days of data, demonstrates the high potential of this low-background detector to discover Galactic WIMP dark matter.

We gratefully acknowledge support from NSF, DOE, SNF, the Volkswagen Foundation, FCT, and STCSM. We are grateful to the LNGS for hosting and supporting the XENON program. We acknowledge the participation of A. Manalaysay (UZH), T. Bruch (UZH), and K. Lung (UCLA) in this analysis.

* guillaume.plante@astro.columbia.edu

- [1] E. Komatsu et al. (WMAP), *Astrophys. J. Suppl.* **180**, 330 (2009).
- [2] G. Bertone, D. Hooper, and J. Silk, *Physics Reports* **405**, 279 (2005).
- [3] J. Angle et al. (XENON), *Phys. Rev. Lett.* **100**, 021303 (2008).
- [4] A. Lansier et al., *Nucl. Instrum. Methods* **135**, 47 (1976).
- [5] E. Aprile et al. (XENON) (2010), arXiv:1001.2834.
- [6] E. Aprile et al., *Phys. Rev. Lett.* **97**, 081302 (2006).
- [7] E. Aprile et al., *Phys. Rev. C* **79**, 045807 (2009).
- [8] A. Manzur et al., *Phys. Rev. C* **81**, 025808 (2010).
- [9] F. Arneodo et al., *Nucl. Instrum. Methods A* **449**, 147 (2000), D. Akimov et al., *Phys. Lett. B* **524**, 245 (2002), E. Aprile et al., *Phys. Rev. D* **72**, 072006 (2005), V. Chepel et al., *Astropart. Phys.* **26**, 58 (2006).
- [10] P. Sorensen et al. (XENON), *Nucl. Instrum. Methods A* **601**, 339 (2009).
- [11] T. Doke, *Nucl. Instrum. Methods* **196**, 87 (1982).
- [12] Z. Ahmed et al. (CDMS II), *Science* **327**, 1619 (2010).
- [13] R. Trotta et al., *J. High Energy Phys.* **12**, 024 (2008).
- [14] C. E. Aalseth et al. (CoGeNT) (2010), arXiv:1002.4703.
- [15] C. Savage et al., *JCAP* **0904**, 010 (2009).
- [16] F. Donato, N. Fornengo, and S. Scopel, *Astropart. Phys.* **9**, 247 (1998).